GRIBBOT – Robotic 3D vision-guided harvesting of chicken fillets

Ekrem Misimi*[1], Elling Ruud Øye[1], Aleksander Eilertsen[1], John Reidar Mathiassen[1], Olav Berg Åsebø[2], Tone Gjerstad[2], Jan Buljo[2], Øystein Skotheim[3]

1. SINTEF Fisheries and Aquaculture, NO- 7465 Trondheim, Norway

2. SINTEF Raufoss Manufacturing, NO- 7465 Trondheim, Norway

3. SINTEF ICT Optical Measurement Systems and Data Analysis, NO-0314 Oslo, Norway

* Corresponding author: ekrem.misimi@sintef.no, Tel.: +47 982 22 467

18   *Abstract*

19   In Norway, the final stage of front half chicken harvesting is still a manual operation due to a lack

20   of automated systems that are suitably flexible with regard to production efficiency and raw

21   material utilisation. This paper presents the 'GRIBBOT' – a novel 3D vision-guided robotic

22   concept for front half chicken harvesting. It functions using a compliant multifunctional gripper

23   tool that grasps and holds the fillet, scrapes the carcass, and releases the fillet using a downward

24   pulling motion. The gripper has two main components; a beak and a supporting plate. The beak

25   scrapes the fillet down the rib cage of the carcass following a path determined by the anatomical

26   boundary between the meat and the bone of the rib cage. The supporting plate is actuated

27   pneumatically in order to hold the fillet. A computer vision algorithm was developed to process

28   images from an RGB-D camera (Kinect v2) and locate the grasping point in 3D as the initial

29   contact point of the gripper with the chicken carcass for harvesting operation. Calibration of

30   camera and robot was performed so that the grasping point was defined using 3D coordinates

31   within the robot's base coordinate frame and tool centre point. A feed-forward Look-and-Move

32   control algorithm was used to control the robot arm and generate the motion trajectories, based on

33   the 3D coordinates of the grasping point as calculated from the computer vision algorithm. The

34   results of an experimental proof-of-concept demonstration showed that GRIBBOT was successful

35   both in scraping the carcass, grasping chicken fillets automatically and in completing the front

36   half fillet harvesting process. It demonstrated a potential for the flexible robotic automation of the

37   chicken fillet harvesting operation. Its commercial application, with further development, can

38   result in automated fillet harvesting, while future research may also lead to optimal raw material

39   utilisation. GRIBBOT shows that there is potential to automate even the most challenging

40   processing operations currently carried out manually by human operators.

41   *Keywords: robot, harvesting, camera, Kinect v2, 3D vision-guided, flexible automation, 3D imaging,*

42   *gripper, chicken, calibration, look-and-Move, visual servoing*

1 Introduction

The poultry processing industry is enjoying worldwide growth in spite of operating on small margins. Processors have faced challenges both in terms of the continued growth of the poultry market and increasing demands from retailers for new and higher quality products. One way of meeting these challenges has been to automate processing operations with the aim of achieving consistently high quality and reducing production costs. In comparison with the fish and some other processing industries, poultry processing is highly automated with the exception of certain challenging operations that are still carried out manually due to the absence of technologies that can compete with the effectiveness of human operators.

Yield is crucial to most producers in the poultry processing industry (Itoh et al. 2009), but existing commercial systems continue to suffer from low product yield compared to established manual operations. A typical operation in poultry processing is the front half deboning of chicken breasts to produce fillets. Automation has been extremely difficult due to the complexity of the operation and the degree of dexterity required. Commercially available deboning systems (Zhou et al., 2007) consist of fixed mechanical technologies that are unable to cope with the wide variations in the sizes and shapes of birds, which consequently renders them unable to optimise raw material yield and utilisation.

In Norway, poultry processing is a massive industry with a production volume of 63,762 metric tonnes and total revenues of NOK 5 billion (approx. USD 1 billion) (Flesland & Hansen 2015). Global annual production is estimated to be 92.7 million tonnes, generating revenues of USD 132 billion. The USA is the industry leader with an annual production of 17.04 million tonnes and revenues of USD 24 billion (FAO, 2012). The industry is dissatisfied with current commercial automated chicken harvesting technologies because, despite of the advantages of these machines, they still cannot compete with the skill, flexibility and adaptability of human operators. Chicken fillets represent the highest-earning product from the entire bird and there is a pressing need from

68   the processing industry to introduce an automated front half fillet harvesting technology that can

69   adapt to anatomical variation, while at the same time optimising raw material utilisation. Norway,

70   in particular, is a specific country given very high labours costs compared to other countries. For

71   industry, a strong incentive for automation of harvesting operation is to make the processing

72   plants more competitive and profitable. Recruitment of qualified labour force is also seen as one

73   of the major challenges in food processing sector. Automation is, therefore, often seen as a

74   measure that can contribute to compensate for the shortage of qualified labour force (Paluchowski

75   et al. 2015).

76   Traditionally, the harvesting of chicken fillets is based primarily on two methods:

77   a) manual harvesting of fillets from the carcass preceded by a cutting operation using a knife or

78   similar cutting tool.

79   b) a fixed machine-based operation using a knife or similar cutting tool combined with a

80   mechanical system designed to release the fillets from the carcass.

81   Many poultry processors employ the manual approach today. Human operators use their visual,

82   tactile and kinesthetic senses, as well as their learning abilities and cognitive skills, to make

83   accurate calculations of the effort required to perform the chicken fillet harvesting operation.

84   The main challenge facing the development of an efficient automated harvesting technology for

85   chicken fillets is to design and build in adaptability to the variations in the size, shape and

86   orientation of the fillets attached to the carcass. These variations require precise identification of

87   the grasping point and adaptive harvesting by means of an effective *grasp*, *scrape and release*

88   procedure. As in other food processing sectors (Balaban et al. 2015), the poultry processing

89   industry is looking for flexible automated solutions that can both automate manual operations but

90   also improve raw material utilization.

91   Robotic automation has been employed in the meat, chicken and seafood industries worldwide,

92   and has included the development of specific gripper tools (Buckingham et al., 2001; Itoh et al.,

93   2009; Bondø et al., 2011; Caldwell, 2012; Purnell, 2013; Purnell, 2006; McMurray et al., 2013;

94   Buljo et al., 2013; Hinrichsen, 2010). For example, robots have enabled increased speeds of meat

95   processing operations, but have so far been unable to adapt to anatomical variations (Barbut

96   2014). Guire et al. (2010) studied the feasibility of robot-based applications using vision or force

97   control for cutting beef carcasses and the harvesting of pork hams. Firstly, they examined the

98   expertise of human operators and studied their manual dexterity during the cutting operation.

99   Subsequently, they tried to replicate this process using an industrial robot. The authors concluded

100 that the main challenge lies in building-in adaptation to the high variability in the size of beef

101 carcasses. As regards chicken, Zhou et al. (2007) reported a study designed to automate front half

102 deboning to produce high-quality chicken fillets. The authors initially studied the structure of the

103 chicken shoulder joint as a starting point for the specification of cutting locations and trajectories,

104 and proposed a 2-DOF (Degrees of Freedom) cutting mechanism. In Zhou et al. (2009), the

105 authors subsequently focused on the kinematics of this cutting mechanism and the accuracy of the

106 actual cutting point location. Hu et al. (2012) describe ongoing work in the intelligent automation

107 of bird deboning and conceptualised the operation in three parts; 1) a characterisation of non-

108 uniform bird anatomy using statistics and image processing, 2) the derivation of a nominal cutting

109 path using image features correlated with internal anatomical structures and robot kinematics, and

110 3) the making of corrections for deviations from the nominal cutting path. The authors concluded

111 that while preliminary results showed that the deboning operation was effective, the cutting robot

112 should be upgraded to incorporate more degrees-of-freedom in order to enable greater versatility

113 in performing the various cuts required for complete bird deboning.

114 One of the key reasons why the use of robotics for automated food handling and processing

115 operations remains a challenge is the difficulty in replicating the complex manual dexterity of

skilled human operators. Consequently, one of the most challenging aspects of implementing robotic automation is the selection and design of the appropriate gripper and cutting tools used to manipulate the raw material. Seliger et al. (2007) and, more recently, Fantoni & Santochi (2014), have described the most commonly applied physical principles for the gripping of non-rigid objects. However, one thing remains clear: there is currently still no universal gripper system for manipulating food raw materials, and the most common approach remains to tailor an optimal system on a case-by-case basis. Pettersson et al. (2011) described a gripper system based on the two-finger principle with emphasis on the hygienic design of the driving mechanism and the force control of fingers against the surface of the food object. Lien & Gjerstad (2008) described a gripper based on the freeze-plate principle, whereby a Peltier element is used rapidly to freeze a gripper plate, thus enabling it to grip the object. By changing the direct current direction, the plate is then re-heated and the object released from the gripper. Gjerstad et al. (2006) designed a compact needle gripper that employed curved needles which penetrated the muscle tissue. This gripper is characterised by excellent grip and clamping force, and was tested on salmon, white and other fish, beef and pork meat with promising results. Sam & Nefti (2010) demonstrated a flexible gripper designed to manipulate a variety of food products based on a combination of the Bernoulli-principle and finger concept. It was tested for the handling of strawberries with promising results. Alric et al. (2014) presented a robotic meat cutting system based on vision and the use of a knife held by one 6-DoF ADEPT Viper robot. A four-fingered gripper was attached to a second ADEPT robot which held the meat being cut. Hu et al. (2012) employed a knife equipped with a force sensor and attached to a 2-DoF robot arm for deboning chicken carcasses.

Our focus in this paper is to present the research resulting in the "GRIBBOT", a novel concept for the robotic harvesting of chicken fillets guided by 3D vision. The name is taken from "*gribb*", the Norwegian term for vulture. The paper includes a proof-of-concept demonstration of a compliant gripper that grasps the fillet, scrapes the carcass, and finally releases the fillet from the carcass.

141 GRIBBOT is a completely novel concept for the robotic automated harvesting of front half

142 chicken fillets. Commercial automation of this operation will not only increase production

143 capacity and profitability in the poultry industry, but may also enable increased utilisation of the

144 raw material at an early stage in production process. The results of this proof-of-concept exercise

145 demonstrate that GRIBBOT has huge potential in terms of the robotic automation of chicken fillet

146 harvesting, and similarly of other challenging food processing operations currently performed

147 manually by human operators. GRIBBOT, with the current configuration, can harvest only one

148 front half fillet at a time.

2   Materials and methods

149

150 GRIBBOT is a 3D vision-guided robotic concept for chicken fillet harvesting consisting of a 3D

151 vision subsystem for the acquisition of RGB-D images, a robot arm for manipulation, a gripper

152 for harvesting and a transport system used to present the chicken carcasses to the GRIBBOT.

153

2.1   Raw material testing

154

155 The chicken carcasses used for research and development of the GRIBBOT were purchased in

156 batches from the Nortura processing plant (Nortura Hærland, Nortura SA) at Økern in Norway

157 over the course of the GRIBBOT's development. The research and development trials of the

158 GRIBBOT were carried out during a period of 15 months. For the final proof-of-concept

159 demonstration, 20 skinless and mechanically-incised chicken carcasses were shipped to SINTEF's

160 PIR (Processing, Imaging and Robotics) laboratory in Trondheim, Norway. Mechanical incision

161 for initializing cut precedes the operation of manual harvesting in poultry processing plants in

162 Norway. The temperature in the lab when performing the research trials was 20 degrees Celsius.

163

164

2.2 In-depth study of manual harvesting

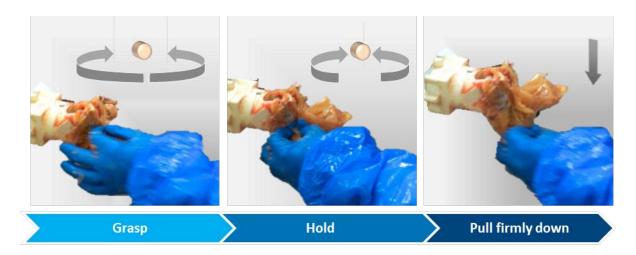166 In Fig. 1 are shown the steps preceding the manual harvesting operation by skilled human

167 operators. Firstly, the operators manually hang carcasses on the cone elements to fix them for the

168 initializing cutting. Then carcasses go into a fileting machine, which makes an initializing cut on

169 the tip of the front half fillet to release them a bit from a carcass. Carcasses coming out of the

170 fileting machine have front half fillets in a slightly hanging position. Subsequently, human

171 operators use their hands to grasp these fillets, and drag them downwards to harvest them.

172 During this operation, human operators use their visual sense to identify and orientate the chicken

173 fillet on the carcass, and the dexterity of their hands and fingers as actuators to fix, capture and

174 harvest the fillet in accordance with the anatomical geometry of the carcass. Visual and tactile

175 feedback allows humans to perform a harvesting operation that is fully adapted to the birds'

176 anatomical variations. The Nortura processing company in Norway employs between 8 and 12

177 operators, working 8-hour shifts, to perform the manual harvesting operation. Using two shifts

178 per day, Nortura's production line processes approximately 50,000 carcasses a day. The weight

179 and size of the carcasses can variate from batch to batch, but a typical average carcass weight is

180 1180 gr, and a mean on weight standard deviation is 200 gr (Bleie 2015). For the sake of clarity,

181 in Norway, a chicken fillet is a skinless and boneless chicken breast, and this terminology with be

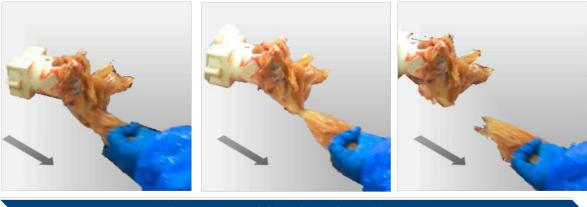182 used throughout the paper.

183

Figure 1. Stages in the manual harvesting of front half chicken fillets, preceded by manual in-feed, mechanical incision for the initializing cut by a fileting machine, succeeded by manual harvesting.

However, in order to develop a robust robotic system for chicken fillet harvesting, we first had to make an in-depth study of the way in which human operators carry out the same operation. We recorded and analysed the basic manual techniques used with an emphasis on motion paths and fillet grasping techniques. The aim of this analysis was to enable us to translate the motion and grasping patterns used by humans into robotic motion trajectories as a basis for the design of an adaptive gripper tool. Studying human operators also allowed us to identify the constraint parameters linked to harvesting that had to be taken into consideration during research and development of the GRIBBOT. The combination of human arm motion and hand grasping patterns defined manual harvesting as a complex operation performed with almost rhythmic versatility. Human operators employed a similar pattern of movement during all harvesting operations. They would first gently approach the fillet and grasp it. Once they were sure that they had a firm grip, they would perform a determined downward tugging or dragging movement, following the contours of the rib cage. Our in-depth study revealed that we had to take the following major considerations into account as part of development of the GRIBBOT's

200　functionality (Figure 2); 1) the grasping and holding of the fillet, 2) a scraping motion using the

201　fingers down the rib cage of the carcass (to make sure that the inner part of the fillet is harvested),

202　and 3) a downward dragging motion that finally releases the fillet from the carcass. Scraping the

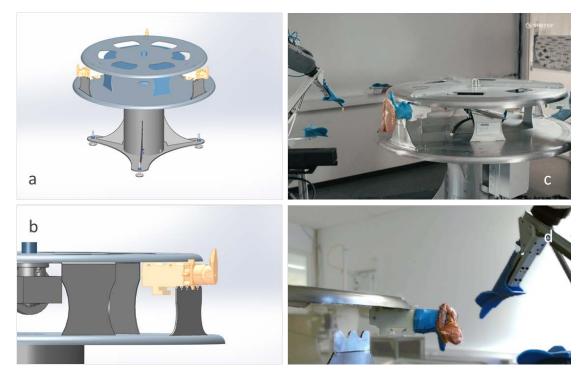203　rib cage was identified as an essential part of the harvesting operation.

204

205　**Figure 2. Complete breakdown of the distinctive motion patterns employed by human operators during harvesting.**

206　## 2.3　Transport system

207　In order to present a chicken carcass to the camera for imaging, and to the GRIBBOT for

208　harvesting, a rotating transport system (TS) was designed and built in stainless steel. Figures 3a

209　and 3b are schematic CAD drawings of the transport system, while the photos in Figures 3c and

210　3d show how the system is used to present the carcass. Three cone elements were mounted on a

rotating plate, and were used to hook the carcass onto the plate and fix its position. The plate was

actuated using an asynchronous low voltage IE1 type three-phase motor of IP55 protection grade

(manufactured by Hoyer in Denmark), and a limit switch with rotary actuation (manufactured by

Osiswitch, Schneider in Germany). Initially, a carcass was manually mounted and positioned onto

the hook of one of the cone elements as shown in Figures 3c and 3b. A signal was then sent to

actuate the plate causing the hook of the cone element to be rotated mechanically by 180 degrees,

thus presenting the carcass to the GRIBBOT. After harvesting, the plate was again actuated and

the cone element returned to its original position, after which the harvested carcass was removed

manually from the hook on the cone element. This constituted one full rotation of a rotating plate

fitted with three cone elements.

Figure 3. Schematic CAD drawings of the transport system (a and b). Transport of chicken carcass by rotation (c), prior to presentation of the front half fillet to the GRIBBOT for image acquisition and manipulation (d).

2.4 Robot Vision
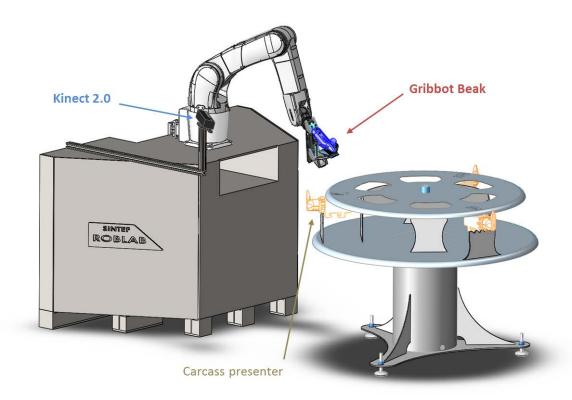
The visual subsystem of the GRIBBOT consisted of a Microsoft Kinect for Windows v2 RGB-D camera. Kinect v2 consists of an infrared/depth camera with an imaging resolution of 512×424 (depth resolution of 3-5 mm and operating range of 0.5-4.5 m) and an HD (High Definition) colour camera with a resolution of 1920×1080. The Kinect v2 depth sensor is based on the time-of-flight (ToF) measurement principle, by which strobed infrared light is reflected by obstacles and the ToF for each pixel recorded by the infrared camera. The depth, or distance (D), in ToF cameras is calculated from the time delay between the emission of a light pulse and its detection by a reflected light sensor:

$$D = \frac{c * \Delta T}{2} \tag{1}$$

where c is the speed of light (constant) and ΔT the measured time delay between light emission and detection of the reflection by the sensor. Since the light pulse travels this distance twice, the product $c * \Delta T$ is divided by 2. The Kinect v2 sensor was fixed to an aluminium profile rod which was bolted onto the robot arm platform. The Kinect v2 camera was connected to a Windows PC via a USB 3.0 communication interface which was installed with the Kinect Software Development Kit (SDK) for Windows. The spatial positioning of the Kinect v2 sensor in relation to other subsystems of the GRIBBOT can be seen in Figures 4 and 5. Several positions of the Kinect v2 sensor were considered, and it was decided that the grasping point would be best determined from a position providing a lateral/perpendicular view of the chicken carcass (Figure 4). The distance between the Kinect v2 sensor and the cone element holding the carcass was 110 cm, while its position on the rod was 122 cm above ground level and 24 cm above the robot platform on which the rod was mounted. Illumination in the lab during research trials consisted of standard indoor fluorescent lighting and closed curtains to prevent direct exposure of the carcass to sunlight, so as to minimise any potential specular reflections from the carcass and cone

250 element. Initial trials were performed using a Microsoft Kinect v1 camera, but image quality was

251 regarded as unsatisfactory and we employed a Kinect v2 instead.

252

253

254 **Figure 4. Spatial positioning of the GRIBBOT subsystems and GRIBBOT overview**

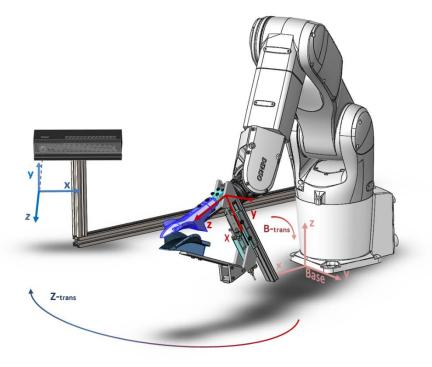255 The chicken carcass RGB and depth (D) images were obtained from the Kinect v2 camera using a

256 LabVIEW-based toolkit developed by SINTEF using the Kinect v2 .NET interface. LabVIEW is

257 manufactured by National Instruments in Austin, Texas, USA.

258 **2.4.1   Camera and robot calibration**

259 Our Kinect camera was mounted at a fixed location in the workplace, and positioned on the robot

260 platform so that it provided a direct view of the chicken carcass (Figure 4). The camera was used

261 in the so-called 'eye-to-hand configuration' in which it adopts a fixed position and orientation in

262 the workspace in relation to the base frame of the robot arm (Siciliano et al. 2007). In our eye-to-

263 hand configuration, the camera's field of view remained static during the harvesting operation.

264 The coordinate frames of the eye-to-hand configuration are illustrated in Figure 5.

265 In order to use features extracted from the Kinect v2 point clouds to control the robot, we decided

266 to apply a coordinate transform approach so that the point clouds could be measured relative to

267 the robot's base frame. The numerous automatic methods used to estimate this unknown

268 coordinate transform (Tsai and Lenz, 1989; Park, 1994; Dornaika and Horaud, 1998) are typically

269 based on a series of measurements of a known calibration pattern. This process is commonly

270 referred to as 'hand-eye calibration'. In the case of our eye-to-hand configuration, once the

271 camera and robot arm are calibrated, the transformation from the camera frame to the robot's base

272 frame remains constant.

273

274 **Figure 5. Coordinate frames in GRIBBOT for the eye-in-hand configuration and calibration based on $A_i X = Z B_i$ equation. X-**

275 **is a transform from Tool Center Point (TCP) to Chessboard frame. A is a transform from chessboard frame to camera frame,**

276 **B is a transform from TCP to base frame, and Z is a transform from base frame to camera frame.**

14

277   Our system was calibrated based on the method described in Tsai and Lenz (1989). A planar

278   calibration board fitted with a printed chessboard pattern was attached to the robot's end-effector

279   flange and a series of images are captured using the Kinect v2 RGB camera (Figure 6). The

280   calibration board defines a coordinate (chessboard) frame in which the X- and Y-axes run

281   horizontally and vertically along the squares, respectively, with the Z-axis oriented perpendicular

282   to the plane of the board (Figure 6). The Kinect v2 camera was assumed to be located at a fixed,

283   but unknown, position with respect to the robot's base frame.

284   **Figure 6.** Examples of images of the calibration board used for eye-to-hand calibration of the Kinect v2

285   The following equation forms the basis for the hand-eye calibration:

286
$$A_i X = Z B_i \tag{2}$$

287   On the left hand side of this equation, X corresponds to transformation from the robot's tool

288   centre point (TCP) to the chessboard frame, and A_i to the transformation from the chessboard

289   frame to the camera frame. On the right hand side, B_i corresponds to the transformation from the

290   TCP to the robot's base frame, and Z to the transformation from the robot's base frame to the

291   camera frame. All the transformations can be expressed as 4x4 matrices describing rigid body

292   transformations, i.e. a rotation followed by a translation. X and Z are fixed, unknown

293   transformations, while A_i and B_i are contingent on the position and orientation of the robot's

294   TCP. All homogeneous matrices in equation (2) are, therefore, of the same form:

295
$$\begin{pmatrix} \mathbf{R} & \mathbf{T} \\ \mathbf{0} & \mathbf{1} \end{pmatrix} \tag{3}$$

296   where R is a 3x3 rotation matrix and T is a translation vector.

297   A_i can be estimated by capturing a set of images and applying standard camera calibration theory

298   to estimate the extrinsic parameters of the Kinect v2 camera. B_i is usually obtained from the

299   forward kinematics of the robot or by reading the position (X, Y, Z) and orientation (Rx, Ry, Rz)

300   of the TCP in robot base coordinates using the DENSO teaching pendant. In our approach, we

301   used the latter.

302   The equation (2) can be solved by passing in a number of known matrices A_i and B_i (typically 10

303   or more) and solving simultaneously for X and Z. Alternatively, X can be eliminated by setting up

304   equation $A_i X = ZB_i$ in the following form:

309

305    $$X = A_i^{-1} ZB_i \qquad (4)$$

306    $$A_{i+1} X = ZB_{i+1} \qquad (5)$$

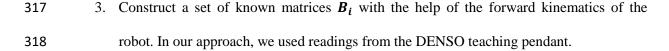307 $$A_{i+1} A_i^{-1} ZB_i = ZB_{i+1} \qquad (6)$$

308    $$A_{i+1} A_i^{-1} Z = ZB_{i+1} B_i^{-1} \qquad (7)$$

310   This is an equation of the form $A_i^* Z = ZB_i^*$, where $A_i^* = A_{i+1} A_i^{-1}$ and $B_i^* = B_{i+1} B_i^{-1}$.

311   The calibration procedure we used was as follows:

312   1. Attach a planar calibration plate to the robot's end-effector. The plate consists of a

313   10mm-thick KAPA Fix® board with a printed chessboard comprising a 10 by 7 pattern

314   of 30x30 mm black and white squares.

315   2. Move the robot's end-effector to occupy a set of 10 or more fixed positions and

316   orientations.

317   3. Construct a set of known matrices B_i with the help of the forward kinematics of the

318   robot. In our approach, we used readings from the DENSO teaching pendant.

4. For each position of the robot's end-effector, capture an image of the calibration plate using the Kinect v2 RGB camera. We used the RGB camera for calibration because it produced better images and resolution than the depth camera.

5. Calibrate the intrinsic parameters of the Kinect v2 camera by passing in all the images of the chessboard pattern and using standard camera calibration functions from the OpenCV library (Zhang 2000, Bouguet MCT).

6. Estimate the position and orientation of the calibration plate in each position and construct the matrices A_i using the *solvePnP()* function from the OpenCV library.

7. Construct the matrices $A_i^* = A_{i+1}A_i^{-1}$ and $B_i^* = B_{i+1}B_i^{-1}$ and use the set of equations $A_i^* Z = Z B_i^*$ to estimate Z based on the *calibrationTsai()* function in the VISP library. This function is based on the algorithm described in Tsai and Lenz (1989).

Matrix Z^{-1} corresponds to the transformation from the Kinect v2 RGB camera to the robot's base frame.

It should be noted that the origin of the Kinect v2 coordinate frame (camera space) is located in the centre of the D-depth camera (the red frame in Figure 7). This is because the point clouds from the Kinect v2 are measured relative to the D-depth, and not the RGB, camera frame. We have compensated for this by measuring the fixed distance (5 cm) between the D-depth and the RGB camera (Kinect calibration) along the X-axis, which conforms to the findings reported by Yang et al. (2015). In addition, it appeared that the *CoordinateMapper()* utility in the Kinect v2 SDK provides points with coordinates that have their origin "inside" the D-depth camera. Empirically, we realised that it was necessary to compensate for this using additional offsets along the X- and Z-axes, and we found that an offset of 5 cm along the X-axis and -1 cm along the Z-axis seemed to work well. We believe that this is due either to an offset in the positions of the in-built cameras or a difference in their focal lengths.

343   The original images taken directly from Kinect v2 are mirror images. For this reason, the X-axis

344   should be viewed from the opposite direction to the depth image. Thus, to ensure that our work

345   was carried out using correct, and not mirror, images, we transformed the point cloud coordinates

346   before they were sent to the *CoordinateMapper()* utility. The transformation was achieved by

347   rotating the original frame 180º about the camera's Z-axis. The result for the Kinect v2 is the blue

348   coordinate frame in Figure 7 – the implication being that the point coordinates from the Kinect v2

349   camera along the X and Y-axes must change sign before multiplication with the transformation

350   matrix $T = Z^{-1}$:

351
$$\begin{pmatrix} X_C \\ Y_C \\ Z_C \\ 1 \end{pmatrix} \tag{8}$$

352   are the coordinates of the point from the Kinect v2 camera as given by *CoordinateMapper()* in

353   metres (m)

354
$$P_{GC} = \begin{bmatrix} -X_C \\ -Y_C \\ Z_C \\ 1 \end{bmatrix} + \begin{bmatrix} -0.050 \\ 0.0 \\ -0.010 \\ 0 \end{bmatrix} \tag{9}$$

355   where, P_{GC} is the so-called grasping point in camera coordinate frame. The 3D coordinates of the

356   point in space (8) are further adjusted in (9) to reflect the compensation carried out for the relative

357   positions of the RGB and D-depth cameras as described above. The grasping point P_G is then

358   defined within the robot coordinate base frame by multiplication with the transformation matrix

359   **T**:

360

361
$$P_G = TP_{GC} \tag{10}$$

362

2.4.2 Computer vision algorithm and calculation of the grasping point

366 Figure 8a shows a schematic diagram illustrating the computer vision operations leading to

367 calculation of the grasping point, which is the initial contact point of the gripper with the chicken

368 carcass. Both Kinect v2 RGB and D-depth images were used during these operations. Firstly, the

369 rectangular ROI-tool in LabVIEW was employed to select the region of interest within which the

370 chicken carcass could appear in the depth image. This enabled image analysis to be focused only

371 on the carcass. The ROI size was selected to be large enough to accommodate anticipated

372 variations in carcass size, and small enough to exclude extraneous elements in the 3D image

373 workspace, such as transport system or other object in the field of view of Kinect v2, that might

374 interfere with the analysis. It was an advantage here that the carcass occupied a fixed location,

375 mounted on the cone elements of the transport system. The rectangular ROI was set manually and

376 could not be changed while the program was running. The depth image taken from the ROI image

377 was then range-thresholded, using the IMAQ Threshold function in LabView, in order to obtain a

19

378   binary mask to be used for segmentation of the carcass and the cone element from the

379   background. Since the accurate segmentation of only chicken carcass required combination of

380   colour RGB image and D-depth image (segmentation from the cone element), the generated

381   rectangular ROI depth image was then enriched with colour information using pixels from the

382   RGB image in the same ROI range. The binary mask, generated from B-blue channel, was

383   applied to the now combined colour and depth image, in order to segment only the carcass. The

384   image was then subjected to shape analysis, first by identifying the width of the carcass i.e. the

385   leftmost and rightmost point of the carcass by width analysis of the carcass, which are marked

386   with red lines by the algorithm in Fig. 8a. Subsequently, we extracted a shape feature from three

387   vertical depth profiles selected along the column dimension of the carcass image. A depth profile

388   here consists of depth values found along one column dimension of the depth image. These three

389   profiles were then used to calculate a single average profile and from this, the maximum depth

390   along the Z-axis in the camera frame was found (see Fig. 8a), i.e. the furthest point from the

391   camera in Z-direction. Mathematically, if D(Z) is a profile function with Z-depth as a variable

392   then:

$$P_{GC} = \underset{Z}{argmax}\ D(Z) = \{Z: D(Z) = Max\} \qquad (11)$$

394   where P_{GC} is the grasping point (initial contact point) in camera frame coordinates (see Fig. 8a).

395   Having calibrated the camera and robot, the grasping point P_G in robot frame coordinates was

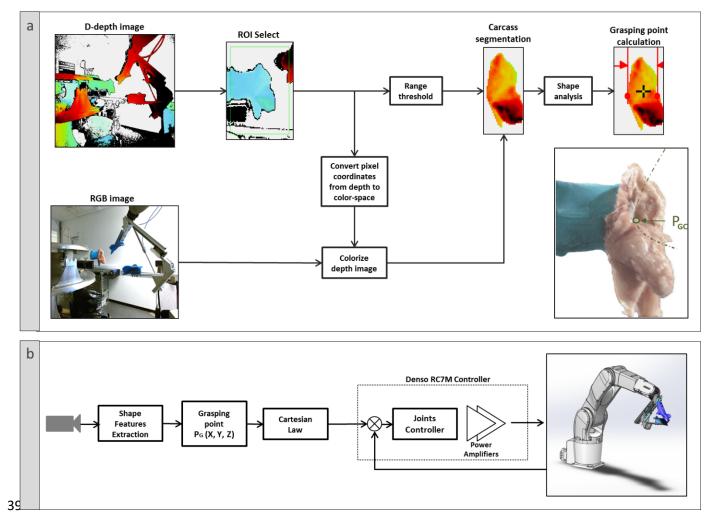396   calculated according to equation (10).

Figure 8. a) RGB-D images of a chicken carcass and the sequence of image processing operations in the computer vision algorithm leading to calculation of the grasping point P$_{GC}$ in camera frame; b) the _Look-and-Move_ control scheme for robotic harvesting.

2.5 Robot arm and control algorithm

The GRIBBOT manipulation subsystem consisted of a base-mounted 6-DoF Denso VS 087 robot arm with industrial protection class IP67. The subsystem is mounted on a steel platform positioned 98 cm above ground level (Figure 4). The arm consisted of 6 revolute joints with a maximum reach of 905 mm and payload of 7 kg, permitting a spherical workplace approximately 1810 mm in diameter. The robot arm control software was written in LabVIEW using functions taken from the relevant library (LabVIEW, Robotics Library for Denso, NI) developed by ImagingLab/Digimetrix (www.imaginglab.it; www.digimetrics.com). All the LabVIEW robot

21

409 commands were sent over an Ethernet connection to the RC7M robot controller. One important

410 function in the robotic library enabled the setting of two different robot speeds (external and

411 internal) within LabVIEW. The key external speed mode enabled us to set different speeds for

412 robot movements in different parts of the motion path. All GRIBBOT subsystems were woven

413 into the LabVIEW environment and controlled from a main program also written in LabVIEW.

414 **2.5.1   Control scheme and trajectory generation**

415 For eye-to-hand configurations, information provided by the camera about the object to be

416 manipulated, such as its environment, 3D localisation and 3D geometry, can be used both for task

417 planning and sensor feedback control (visual servoing, Siciliano et al., 2009). There are two main

418 categories of vision-based control schemes: a) position-based visual servoing (PBVS) and b)

419 image-based visual servoing (IBVS). The main difference is that PBVS schemes use visual

420 measurements to calculate the pose (position and orientation) of the object to be manipulated with

421 respect to the robot arm, while in IBVS schemes the object's image feature parameters are used to

422 compare the current with the desired pose. Both control schemes are used extensively in practical

423 applications (Chaumette & Hutchinson, 2006 and 2007; Lippiello et al., 2007).

424 A diagram of the control scheme is shown in Figure 8b. Our scheme can be best described as a

425 *Look-and-Move* approach (Weiss et al. 1987) in which visual measurements are used as part of a

426 feed-forward process (Pieters et al. 2012). We selected this scheme because it enabled us to

427 optimise the gripper and scrape procedure according to rib cage anatomy. This meant that we

428 didn't have to rely on visual feedback once the grasping point was calculated. Visual feedback

429 was no longer necessary once we had established that eye-to-hand calibration was accurate, and

430 that the carcass was robustly positioned and did not move during manipulation

431 Firstly, shape features were extracted from the camera images, and the coordinates of the

432 grasping point in camera frame were calculated. These coordinates were then converted to robot

433 base frame coordinates according to equation (10). Starting from its '*Home*' position, the arm was

434 then commanded to move the end-effector to the grasping point. The '*Home'* position is defined

435 as a default starting position and orientation prior to harvesting. The movement of the arm along

436 the robot's motion path between the *Home* position $P_H(X, Y, Z)$ and the grasping point $P_G(X, Y,$

437 $Z)$ was achieved according to Cartesian Law using the *Move by Coordinates* VI function in

438 LabVIEW. In order to specify the interpolation path of the end-effector between the *Home*

439 position and the grasping point, one could choose between a default setting (the most efficient

440 path to the next location) and a linear interpolation. We selected a linear approach which exists as

441 an option in the *Move by Coordinates* VI parameter cluster together with the pass motion and

442 move options within the Cartesian coordinate frame. Linear interpolation was selected because it

443 provided greater predictability for point-to-point movement, which was more relevant to our

444 application. The motion path for the entire harvesting procedure can be described by breaking it

445 down into the following segments:

446 1. The aforementioned motion path segment from *Home* position to the grasping point P_G was

447 called the *Approach* path.

448 2. The trajectory for the combined scraping, grasping and holding segments was semi-predefined

449 on the basis of trial and error while manually controlling the robot using a DualShock®3 wireless

450 controller, manufactured by Sony computer entertainment in Minato, Tokyo. This trajectory was

451 then used as a template for the control program. The initial contact point of the robot arm motion

452 with the carcass is given by the grasping point P_G, calculated from the Kinect v2 image according

453 to Eq (10). This point was then compared to the first point in the predefined trajectory (P_{t1}) by

454 calculating the difference (P_{Diff}):

455
$$P_{Diff} = P_G - P_{t1} \tag{12}$$

456   P_{Diff} was then used as an offset value by which to move the coordinates of the points in the

457   predefined trajectory to match the grasping point calculated by the 3D computer vision. However,

458   since the carcass was presented at the same height each time, the Z-values during the motion

459   followed the Z-values of the pre-determined trajectory for the remaining points constituting the

460   *scraping* and *grasping* trajectory (Eq. 14). The new trajectory (P_t) was then as follows:

461
$$P_{t_1} = P_G, \quad for\ the\ first\ point\ (i = 1) \tag{13}$$

462
$$P_{t_i} = \begin{pmatrix} X_i \\ Y_i \\ Z_i \end{pmatrix} + \begin{pmatrix} X_{diff} \\ Y_{diff} \\ 0 \end{pmatrix}, \quad i > 1\ for\ the\ remaining\ points\ in\ the\ trajectory \tag{14}$$

463   The control algorithms made no changes to tool orientation during the trajectory, and the angles

464   from the predefined trajectory were retained. Thus the same tool orientation (R_x = -148°; R_y =

465   29°; R_z = -87°) was used for the entire scraping motion path. After completion the tool rose

466   towards the centre of the carcass and turned to adopt a position that made it easier to grasp and

467   hold the fillet (R_x = -94°; R_y = 43°; R_z = -50°). The fillet was then grasped by actuating the

468   supporting fillet element on the gripper (Figure 9). The tool then turned back towards its initial

469   position, with the final orientation being R_x = -124°; R_y = 38°; R_z = -67°. These segments of the

470   motion path were called *Scrape* and *Grasp&Hold*.

471   3. Motion paths for the subsequent *Pulldown* (a downward pulling motion once the gripper has

472   grasped and clamped the fillet) and *Release* (release of the fillet from the gripper) operations,

473   followed by return to *Home* position, were completed according to the predefined motion
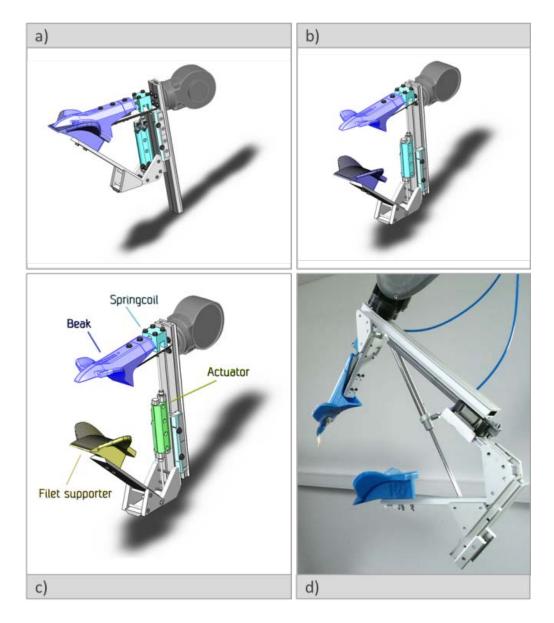
474   trajectories.

475   The external speed of the robot arm during movement along these trajectories was set at 60% of

476   maximum speed. The maximum composite speed of the DENSO VS 087 was reported to be

477   11000 mm/s.

478   ## 2.6   Gripper

2.6.1   Gripper design and actuation

In many robot-based food handling and processing applications, the gripper is an important component and its effective function can be critical to the success or failure of an automated food handling process. The design and development of the GRIBBOT gripper required several iterations. Our key design approach was led by the following principles: a) the gripper should replicate human hand motion patterns used during harvesting, b) the gripper should have a scraper function in order to optimise raw material utilisation and c) the gripper should be equipped with a clamp to hold the fillet and thus facilitate harvesting during the *Pulldown* operation.

The GRIBBOT's gripper is a pneumatic tool equipped with both scraper and clamping functions. The model used in the proof-of-concept demonstration is shown in Figure 9. The gripper was actuated using a cylindrical pneumatic actuator supplied with compressed air at a pressure of 6 bar. The actuator was opened and closed using in-built DENSO robot solenoids controlled via an on/off 24 V signal. A CAD drawing of the gripper is shown in Figure 9c, illustrating its main components including the beak and fillet supporter. Both of these components were 3D-printed in PLA plastic (polyactic acid) at SINTEF's laboratories using a Prusa i3 3D printer, manufactured by RepRap Core Developer Prusajr. Figure 9d is a photograph of the gripper with its 3D printed beak and fillet supporter. We should point out that hygienic design and food safety considerations of the GRIBBOT and its gripper were outside the scope of this study.

Figure 9. CAD model of a pneumatic gripper with scraper function; a) closed state, b) open state, c) gripper components, and d) an image of the gripper working in open state.

The beak's main function was to make first contact with the chicken carcass at the fillet grasping point localised on the basis of 3D computer vision, and to scrape the fillet along the rib cage of the carcass in a way that optimises yield by leaving as little residual meat on the carcass as possible. The beak design was intended to replicate a human thumb and to scrape the fillet meat down the rib cage and release it from its tendon attachments. A spring coil component was fitted in the beak with the following functions: 1) to make the beak compliant during the scraping

26

action of harvesting by enabling it to follow the path defined anatomically by the boundary

between the meat and the bone of the rib cage, 2) to compensate for possible minor deviations in

the Z (depth) direction from the 3D computer vision-calculated grasping point, and 3) to ensure

that the initial contact with the meat is gentle. Both the beak and fillet supporter were designed

with a curved profile to minimise excessive squeezing during harvesting. As shown in Figure 10,

both gripper components are equipped with flaps to increase the area of surface contact with the

fillet and thus facilitate gentle handling. The surface areas of the beak and fillet supporter

(without flaps) were 59.96 cm^2 and 56.5 cm^2 respectively. The corresponding arch angles were

25.2 and 18.73 degrees. Both the beak and fillet supporter were printed with corrugations on their

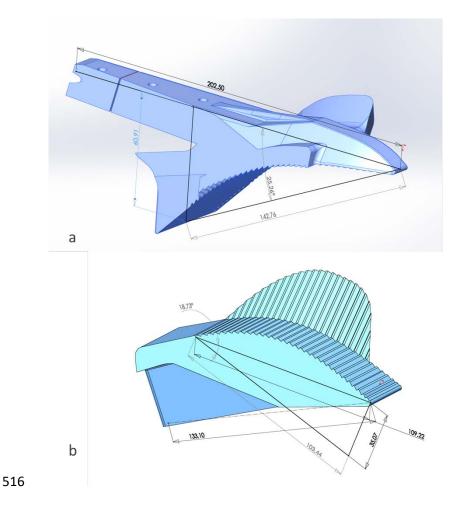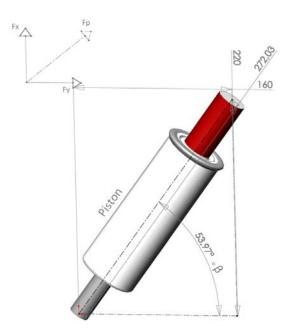contact surfaces in order to enhance friction and grip during harvesting.

2.6.2 Calculation and measurements of gripper impact forces

In order to evaluate the grasping and holding functions performed by the gripper throughout the harvesting operation, it is necessary to calculate and measure the forces exerted on the fillet. This is also essential during assessments of the gripper's impact on the quality of the fillet after harvesting. Calculations and measurements were performed using decomposition of the force exerted onto a piston rod (F_P) into Fx and Fy components along the X and Y directions, respectively. Figure 11 illustrates some important parameters and the geometrical positioning necessary to calculate the gripping force. The piston rod diameter of the pneumatic actuator was measured at 1 cm.

Figure 11. Geometrical illustration of pneumatic actuator positioning and force decomposition, where F_P is the force along the piston rod axis, and Fx and Fy the decomposition forces in the X (between the gripper plates) and Y directions.

533   Measurements of the force applied to the chicken fillet between the two gripper components were

534   performed using a Futek FSH00095 miniature force sensor manufactured by FUTEK in

535   California, USA, which has a capacity range of up to 4.536 kg.

536   **2.6.3   Gripper offset**

537   The eye-to-hand calibration procedure described in section 2.4.1 was carried out according to

538   equation (2), in which ***B*** denoted the transformation from the mechanical interface system

539   (flange) to the robot's base coordinate system. When no tool (end-effector) is attached to the

540   flange, this is actually the Tool Centre Point (TOOL0) given in base frame coordinates (the

541   DENSO TCP, by definition). Whenever a new tool is added, an offset is introduced. The offset

542   must be calculated from the origin of the TOOL0, and this is referred to as the Tool Centre Point.

543   When we mounted the gripper (Figure 9) on the mechanical interface of the robot arm, the TCP

544   requiring calculation was defined as the gripper's 'active point', which in our case was the tip of

545   the gripper's beak. Since there was no difference in orientation (Rx=Ry=Rz=0) between the

546   mechanical interface system frame (TOOL0) and the gripper frame, the TCP could be established

547   simply by calculating the offset by means of translation in the Z-direction (since the gripper is

548   pointing in the Z-direction):

549
$$P_{Off} = \begin{pmatrix} x_{Off} \\ y_{Off} \\ z_{Off} \end{pmatrix} = \begin{pmatrix} 0 \\ 0 \\ 290 \end{pmatrix} \qquad (15)$$

550   Thus, the offset in the Z-direction was 29 cm=290mm. This was calculated using the DENSO

551   teaching pendant, in which we simply defined the gripper as a new tool by setting the measured

552   offset values in the X, Y, and Z directions (Rx=Ry=Rz=0).

553   # 3   Results and Discussion

554   ## 3.1   3D vision and eye-to-hand calibration results

555   The intrinsic parameters of the Kinect v2 camera can be summarised as follows:

556
$$K = \begin{bmatrix} f_x & 0 & c_x \\ 0 & f_y & c_y \\ 0 & 0 & 1 \end{bmatrix} = \begin{bmatrix} 1053.14 & 0 & 958.64 \\ 0 & 1055.54 & 515.68 \\ 0 & 0 & 1 \end{bmatrix} \tag{16}$$

557   where K is the camera matrix with focal lengths in pixels (in both directions), and c_x, c_y are the

558   principal point components.

559   The radial and tangential distortion coefficients were as follows:

560    $[k_1 \, k_2 \, p_1 \, p_2 \, k_3] = [\, 0.038290 - 0.019621 - 0.000011 \, 0.000378 - 0.031097\,]$ (17)

561   The accuracy of the camera calibration was evaluated by computing the root mean squared error

562   (RMSE), whose average in pixels was 0.2468. Table 1 provides a summary of the parameters of

563   the Kinect v2 camera.

564   **Table 1. Results showing the extrinsic parameters of the Kinect v2 camera, where rx, ry and rz are rotational vectors, and Tx,**

565   **Ty and Tz are translational vectors characterising the pose (position and orientation) of the camera frame with respect to the**

566   **base frame.**

Calibration Image #	rx	ry	rz	Tx	Ty	Tz
1	0.639	0.23	-2.89	-0.227	0.0472	0.719
2	0.455	-0.563	2.73	0.251	0.0323	0.754
3	-0.701	0.34	-3.04	0.0845	0.103	0.678
4	1.17	0.291	-2.78	0.0287	0.101	0.801
5	-0.116	0.929	2.81	0.184	-0.0186	0.452
6	0.045	1.17	-2.9	0.104	0.0159	0.931
7	0.0913	0.184	-3.01	0.255	0.102	0.39
8	0.108	0.175	-3.02	-0.174	0.338	0.865
9	0.0384	-0.287	2.56	0.116	0.154	0.792
10	0.386	0.55	2.57	0.0509	-0.0544	0.537

567 Figure 8a displays both RGB and D-depth images, as well as the image resulting from shape

568 analysis of the chicken carcass and the calculation of the grasping point P$_{GC}$ in camera frame. The

569 figure also illustrates how the computer vision algorithm calculated and displayed the carcass

570 boundaries (red vertical lines). The grasping point (P$_{GC}$), calculated according to equation (11), is

571 marked on the carcass-coloured depth image using a cross symbol. The corresponding resulting

572 transformation matrix $T = Z^{-1}$, used for the eye-to-hand calibration, is summarised in Table 2.

573 **Table 2. The T-transformation matrix describing the transformation from the Kinect v2 camera frame to the robot's base**

574 **frame**

$$
\begin{matrix}
0.969591 & 0.00418 & 0.244695 & 0.609527 \\
-0.24458 & -0.01844 & 0.969454 & -0.39838 \\
0.008563 & -0.99982 & -0.01685 & 0.325573 \\
0 & 0 & 0 & 1
\end{matrix}
$$

575

576 The accuracy of the eye-to-hand calibration was evaluated by taking the difference of both sides

577 of the equation $A_i^* Z = Z B_i^*$ for each image of the calibration plate and summarising the positional

578 and rotational residuals (Table 3). The positional residuals are calculated from the translation part

579 of the matrix (column 4, rows 1 to 3), while the rotational residuals are calculated by converting

580 the 3x3 rotational part of the matrix to a rotation vector using Rodrigues' rotation formula

581 (Wolfram, Mathworld). The first column displays the root mean square error (RMSE) in position

582 AZ=ZB, while the second column shows the error in orientation or rotational vector expressed in

583 degrees. The maximum error in position was found to be 13 mm, while the mean error was 6.4

584 mm, and standard deviation 3.8 mm. We performed an additional evaluation of the eye-to-hand

585 calibration by directing the robot arm to move the tip of the gripper (beak tip) to several points

586 calculated using equations (9) and (10). The results of this additional validation revealed a mean

587 accuracy similar to that reported in Table 3. A combination of factors, such as the reported Kinect

588 v2 camera resolution accuracy of 3-5 mm (section 2.4), noise on the depth image due to specular

589 reflections from the chicken fillet and carcass, and the error in the eye-to-hand calibration, all

590 contributed to the mean accuracy of the gripper position at the grasping point. Our experience

591 was that the chicken fillet was an optically challenging object to measure because of specular

592 reflections generated by meat texture and slime. This concurs with Lachat et al. (2015) who

593 assessed the effects of different material properties on the distance (depth) measurement, and

594 showed that for highly reflective materials distances measured with the Kinect v2 camera can

595 vary by up to 6 cm.

596 **Table 3: Summary of results of the evaluation of eye-to-hand calibration performed by calculating the AZ=ZB positional (T)**

597 **and rotational (r) residuals (root mean square error).**

	T (mm)	**r** (degrees)
1	4.4	0.49
2	3.9	0.34
3	3.2	0.19
4	8.6	0.72
5	13.0	0.9
6	11.6	0.93
7	5.4	0.65
8	2.0	0.22
9	5.7	0.61
Mean	6.4	0.56
Std.dev.	3.8	0.27

598 3.2 Robotic grasping and harvesting of chicken fillets

599 Figure 12a provides an illustration of gripper motion paths in the OXZ plane for three different

600 examples of grasping point locations P_{G1}, P_{G2} and P_{G3}, in robot base frame coordinates, which

601 were calculated using the 3D computer vision algorithm shown in Figure 8a and equations (10)

602 and (11). The figure shows that all specific paths are linear (as described in section 2.5.1) from

603 the starting point P_H which is the *Home* position of the robot arm/tip of the gripper. All segments

604 of the motion path are numbered, and the main difference between the segments is that segment 5

605 (black line) represents a predefined motion path, while the other segments were influenced by

606 computer vision localisation of grasping points for different chicken carcasses, as described at the

607   end of section 2.5.1. It should be noted that, although the scrape segments traced by the gripper

608   (denoted as 2 in the figure) are linear, due to the compliancy of the gripper facilitated by the

609   spring coil component, the critical scraping part of the motion path is actually non-linear because

610   the tip of the gripper followed the path determined by the anatomical structure of the rib cage

611   (Figure 12b). This meant that the tip of the gripper followed the boundary between the fillet meat

612   on the one hand, and the ligaments and bones of the rib cage on the other. Thus, while we

613   maintained high levels of predictability for our motion path by using linear interpolation between

614   specific points along the trajectory, we also managed to ensure that the gripper followed the

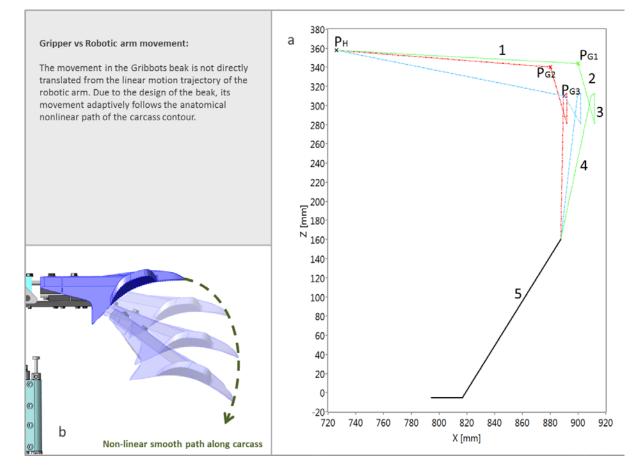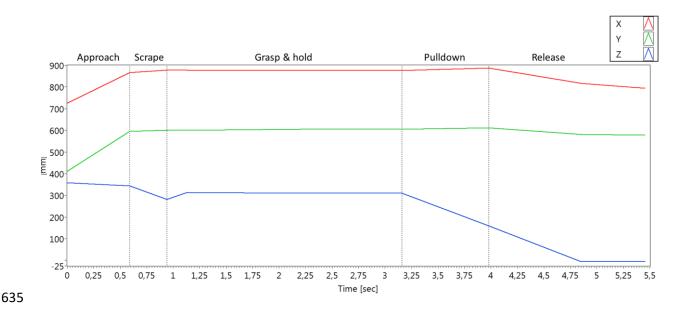615   optimal path during the scraping operation, i.e. the path determined by chicken carcass anatomy.

616

617   **Figure 12. The gripper motion path in the OXZ plane during harvesting for different grasping point positions P_{Gi} (referenced**

618   **to the base frame). Segments of the motion path are numbered as follows: 1-Approach, 2-Scrape, 3-Grasp&Hold, 4-Pulldown,**

619   **5-Release. Segment 5 (Release) is predefined and not affected by 3D computer vision calculations of grasping points.**

620   Timelines for the position trajectory (X, Y and Z coordinates) of the DENSO robot arm are

621   shown in Figure 13. Timelines for the orientation components (Rx, Ry and Rz) are not reported

622   here. The *Approach* phase is completed after about 0.6 seconds. Prior to this phase, while

623   GRIBBOT is in its *Home* position, the 3D computer algorithm is calculating the grasping point.

624   During the *Approach* phase, the GRIBBOT moved towards the localised grasping point and

625   descended vertically in the Z direction from 36 to 35 cm (P_{G1}) where it assumed the grasping

626   pose. When this pose was achieved (P_{G1}), the scraping phase began and was completed before 1

627   second had elapsed. The subsequent *Grasp&Hold* phase thus began at approximately 1 second

628   and was completed after 3.2 seconds. During this phase the pneumatic actuator pushed the

629   supporting element of the gripper upwards and the gripper was closed. Next, the *Pulldown* phase

630   began and was completed after 4 seconds had elapsed. We observed that during *Pulldown,* when

631   the GRIBBOT pulled the fillet downwards, the robot arm lowers the gripper from 32 to 16 cm in

632   the Z direction, while the X and Y positions remain virtually unchanged. The final *Release* phase,

633   during which the pneumatic gripper was opened and the fillet released, began at 4 seconds and

634   ended at 4.75 seconds.

635

636   **Figure 13. Gripper trajectories during the robotic harvesting of front half chicken fillets from the carcass**

637   Figure 14 displays a sequence of images showing the complete robotic harvesting operation of a

638   front half chicken fillet. The *Approach* phase, during which the gripper descends towards the

639   localised grasping point P_G where the tip of the beak makes the initial contact with the fillet, is

640   shown in Figures 14a and 14b. Figures 14c, 14d and 14e show the *Scraping* of the fillet from the

641   rib cage, following the path determined by the anatomical boundary between the meat and bone.

642   Figure 14f illustrates how the robot arm changes its orientation as the pneumatic gripper is

643   actuated to close and thus grasp and hold the fillet between its beak and supporting plate (Figures

644   14g, 14h and 14i). Figure 14i also shows how the robot arm again changes its orientation to

645   initiate the *Pulldown* phase during which the fillet is dragged downwards. The end of this phase

646   marks the completion of the harvesting operation during which the fillet, including the tenderloin,

647   is separated from the carcass. This figure also shows how the robot arm changes orientation to

648   prepare for initiation of the *Release* phase during which the pneumatic actuator opens the gripper

649   plates and the fillet is released. Figure 15a shows the result after harvesting operation of a front

650   half fillet with GRIBBOT. It can be seen that also tenderloin is harvested along with the fillet.
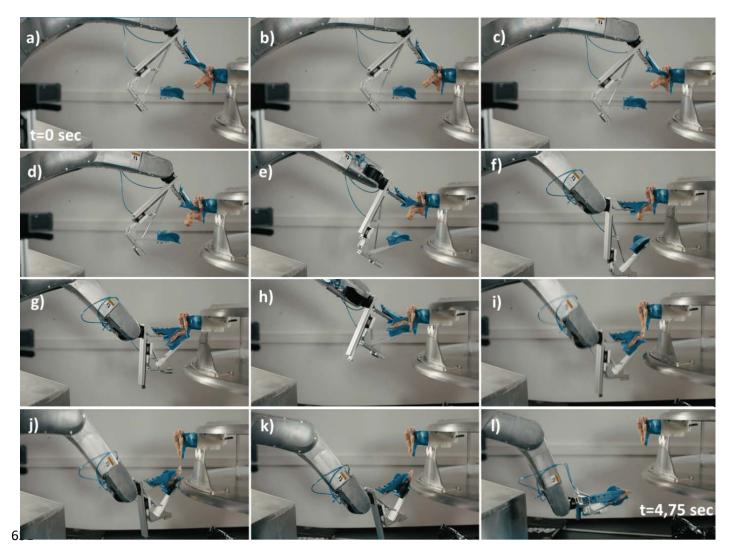
Figure 14. The complete sequence of a robotic harvesting operation of a front half chicken fillet. The entire harvesting operation, from Approach (a) to Release (l) is completed in about 4.75 seconds.

3.3 Gripper impact force on the fillet

For a pneumatic actuator piston rod diameter (d) of 1 cm, and air pressure (P) of 6 bars, the resulting force along the piston rod was calculated as:

$$F_P = P * A = 6 \ bar * \pi r^2 = 600 \ 000 \frac{N}{m^2} * 0.0000785 m^2 = 47.1N \tag{18}$$

The angle (β) was 53.97° (see Figure 11). Thus the gripper force exerted on the fillet between the gripper plates was:

$$F_x = sin\beta * F_P = 38.09N \tag{19}$$

661   The force exerted on the fillet between the gripper plates measured using a force sensor, as

662   described in section 2.6.2, was 39.5 N.

663   We observe that the calculated force exerted on the fillet is within the range of, and in accordance

664   with, the force measured using the force sensor. During the harvesting operation, the gripper was

665   able to grasp and hold the chicken fillet without causing damage or any degradation in quality.

666   Figure 15 shows the effects on a fillet of the grasping and holding phases. At first we see that the

667   corrugations on the inside surfaces of the gripper plates, designed to enhance grip between the

668   plates during harvesting, created visible elastic pattern marks in the front part of the fillet (Figure

669   15c). These marks were reversible and disappeared after 1 minute (Figure 15d), leaving the fillet

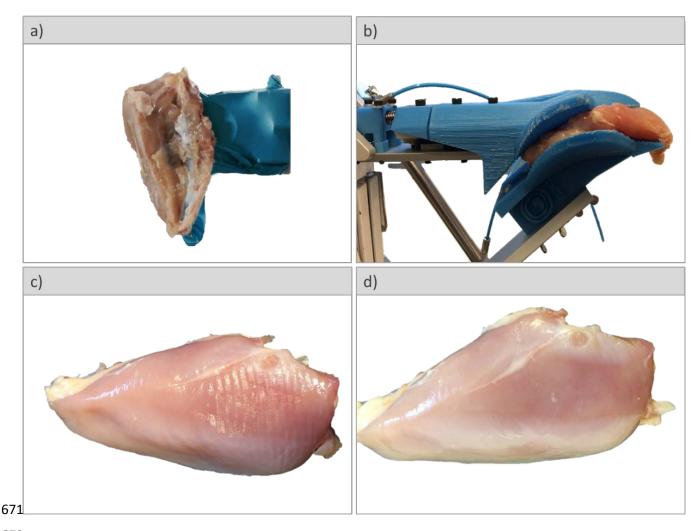670   entirely without any physical damage or degradation in quality.

Figure 15. Result of the harvesting operation with GRIBBOT and effects of the grasping and holding phases on a chicken fillet using a gripper actuated pneumatically by compressed air at 6 bar: a) result of the harvesting with GRIBBOT, b) fillet between the gripper plates in *Hold* position, c) fillet after release from the gripper showing visible corrugation marks on the surface, d) corrugation marks are reversible and disappear after 1 minute.

3.4 General observations and relevance for industrial applications

Further optimisation of harvesting motion trajectories will mean that it is likely that the current time (4.75 sec) it takes to complete the operation can be reduced. This applies specifically to the *Grasp&Hold* (currently 2.2 sec) and *Pulldown* segments, and also to the *Release* process after harvesting. Additional time savings may be achieved by increasing the robot arm's speed from 60 to 100 per cent of maximum, but this is something that needs to be investigated in future research; specifically, how increase of robot speed affects the deformation of chicken meat during the

38

683   scraping and pulldown phase, as the most critical segments of harvesting operation. More

684   investigations are needed to establish knowledge on how much force the chicken fillet can be

685   exerted to during harvesting stages before quality degradation. Gjerstad (2012) calculated the

686   robot arm cycle time needed for packaging of salmon fillet portions taking into consideration the

687   industrial requirements and acceleration limit. The cycle time was found to depend on the force

688   added to the raw material and the quality of the raw material, both of which are reflected in the

689   acceleration limit. Gjerstad (2012) concluded that it is necessary to adjust acceleration levels

690   upon appearance of degradation in texture quality in salmon fillet portions.

691   The mean error and standard deviation (Table 3) in positioning of the gripper, as reported in

692   Section 3.1, did not pose any problems during harvesting. The compliancy of the gripper,

693   facilitated by its spring coil component, was designed to compensate for these small positioning

694   errors (Table 3), and this functioned satisfactorily during our trials.

695   Since the harvesting of front half chicken fillets from the carcass was done in normal indoor

696   ambient light, it is important to point out that the ambient light did not have any significant effect

697   on the computer vision system and detection of the grasping point with Kinect v2 camera. The IR

698   (Infra Red) Kinect v2 camera is very robust regarding the illumination conditions, but the RGB

699   camera is less robust to these variations and specular reflections. We tested this by illuminating

700   the chicken carcass with two powerful halogen lights. While the depth image quality was

701   uninfluenced, we saw that is was necessary to change the threshold value for color segmentation.

702   In addition, we variated illumination from dark to very bright to see the effect in segmentation of

703   the chicken from the cone element. We noted that, compared to RGB channels, Hue channel from

704   HSV (Hue, Saturation, Value) color space, was a robust channel for segmentation of the carcass

705   from the cone element in the image. It is known that, in HSV color space, the brightness

706   (intensity information) is separated from the chrominance (color information) leading to reduction

707   in the effect of uneven illumination (Premaratne 2014). Therefore, Hue channel can be more

708   efficient for segmentation than channels in RGB space when objects are subjected to non-even or

709   varying illumination conditions (Cheng et al. 2001).

710   The main advantage of GRIBBOT's gripper is that it is designed to follow the non-linear path

711   determined by the anatomical boundary between the chicken meat and rib cage bone. The

712   gripping force is spread over a large surface area comprising the gripper beak and fillet supporter,

713   thus ensuring no quality degradation of the fillet after harvesting. Further optimisation of the

714   gripper can be achieved by printing the gripper plates in an FDA-approved food processing

715   material such as PEEK (PolyEtherEtherKetone, OPM, USA). It could also be coated in a thin

716   layer of compliant elastomer to increase flexibility during the *Grasp&Hold* operation. Greater

717   flexibility may also be achieved by mounting tactile elements onto the inner surfaces of the

718   gripper plates to regulate the force exerted on the fillet. Important aspects to address in the future

719   research are the mechanical, optical, textural properties and behaviour of chicken meat in

720   different conditions and temperatures, and investigate the influence of these aspects on the

721   harvesting operation. Investigation of these aspects was outside of the scope of the current study.

722   Harvesting using the GRIBBOT and its constituent components as described in this paper is a

723   strong argument for the benefits of both the eye-to-hand configuration and the *Look-and-Move*

724   control scheme when compared with other approaches. The use of the Kinect v2 camera ruled out

725   the potential use of Kinect in a hand-in-eye configuration because the minimum distance from the

726   object required to acquire depth images using Kinect v2 is 60 cm. An overall evaluation suggests

727   that our approach is close to optimal, given the following results; a) good eye-to-hand calibration,

728   b) robust positioning of the carcass on the transport system's cone elements, and c) an optimal

729   compliant gripper that is directed by anatomy along the rib cage at adequate manipulation speed.

730   Given the trade-off required between accuracy and speed, the *Look-and-Move* scheme provided

731   satisfactory results.

We believe that the GRIBBOT has huge potential for the commercial automation of front half chicken fillet harvesting, and may have a potential for improving efficiency in chicken meat utilisation with further development. There are several reasons why the GRIBBOT, with further development, can be easily integrated into existing production machinery. Firstly, the RGB-D camera used in this application is mass-produced and highly cost-efficient. Secondly, the robot arm has already been assigned an IP protection degree that satisfies food industry applications characterised by periodic equipment washings. Additional developmental steps required to bring the GRIBBOT closer to full commercial use include the issues already described in this Section, combined with close collaboration with a capable technology vendor that can move current development status to a higher Technology Readiness Level.

4   Conclusions

In this paper, we have presented a concept named 'GRIBBOT', designed to carry out the robotic harvesting of front half chicken fillets. Harvesting is a challenging operation and is predominantly carried out manually. The GRIBBOT combines a 3D vision algorithm for calculation and localisation of the grasping point (initial contact point of the gripper with the carcass) using a RGB-D camera (Kinect v2), with a robotic arm fitted with a specially designed compliant gripper. The GRIBBOT succeeded in correctly calculating the 3D coordinates and location of the fillet's grasping point. The motion paths controlling the robot arm, combined with the compliancy of the gripper, enabled the GRIBBOT to scrape the fillet following the path determined by the anatomical boundary between the meat and the carcass' rib cage bone. The result was the successful harvesting of front half fillets, including the tenderloin, from the carcass. The paper includes a proof-of-concept demonstration showing that the entire robot-based harvesting procedure for a single fillet was carried out in less than 4.75 seconds. GRIBBOT is an example of research and technology development with potential for flexible and adaptive robot-based

756 automation in food processing. This is due to adaptivity both with respect to the localisation of

757 the grasping point enabled by a 3D vision algorithm, and in relation to the potential for

758 optimisation of raw material utilisation. We believe that the GRIBBOT has significant

759 commercial potential both in the poultry industry and other food industry applications where

760 flexible robotic automation can contribute to higher levels of production sustainability and bio-

761 resource efficiency. The GRIBBOT demonstrates that there is scope for automating even the most

762 challenging food processing operations.

5 References

770

771 Alric, M., Stephan, F., Sabourin, L., Subrin, K., Gogu, G., Mezouar, Y., 2014. Robotic solutions

772 for meat cutting and handling. In Proceeedings of EWDOM14-European Workshop on

773 Deformable Object Manipulation. Lyon, France.

774 Balaban, M.O., Misimi, E., Alcicek, Z., 2015. Quality Evaluation of Seafoods. In Sun, D.-W.

775 (Ed.) Computer Vision Technology for Food Quality Evaluation, 2nd edition, In Press.

776 Barbut, S., 2014. Review: Automation and meat quality-global challenges. Meat Science. 96(1),

777 335-345.

778   Bleie, O. 2015. Email communication with Olav Bleie at Nortura AS.

779   Bondø, M.S., Mathiassen, J.R., Vebenstad, P.A., Misimi, E., Bar, E.M.S., Toldnes, B., Østvik,

780   S.O., 2011. An automated salmonid slaughter line using machine vision. Industrial Robot: An

781   International Journal 38(4), 399-405.

782   Bouguet, J.Y., MATLAB calibration tool. http://www.vision.caltech.edu/bouguetj/calib_doc/

783   Buljo, J.O., Gjerstad, T.B, 2013. Robotics and automation in seafood processing. In: Caldwell,

784   D.G. (Eds.), Robotics and Automation in the Food Industry. Woodhead Publishing Limited,

785   Cambridge, pp. 329-353.

786   Buckingham, R., Graham, A., Arnarson, H., Snaeland, P., and Davey, P., 2001. Robotics for de-

787   heading fish – a case study. Industrial Robot: An International Journal, 28 (4):302-309.

788   Caldwell, D.G., 2012. Robotics and automation in the food industry: Current and future

789   technologies. Woodhead Publishing.

790   Chaumette, F., S. Hutchinson, S., 2006. Visual servo control, Part I: Basic approaches. IEEE

791   Robotics and Automation Magazine 13(4), 82-90.

792   Chaumette, F., S. Hutchinson, S., 2007. Visual servo control, Part II: Basic approaches. IEEE

793   Robotics and Automation Magazine, 14(1), 109-118.

794   Cheng, H.D., Jiang, X.H., Sun, Y., Wang, J. 2001. Color image segmentation: advances and

795   prospects. Pattern Recognition, 34, 2259-2281.

796   Denso   Tool   Coordinates   System   and   Tool   Definition,

797   http://densorobotics.com/content/user_manuals/19/001967.html, accessed 09.07.2015.

798   Dornaika, F., Horaud, R., 1998. Simultaneous robot-world and hand-eye calibration. IEEE

799   Transactions on Robotics and Automation. 14(4), 617-622.

800   Fantoni, G., Santochi, M. et al. 2014. Grasping devices and methods in automated production

801   processes. CIRP Annals - Manufacturing Technology 63(2), 679-701.

802   FAO, 2012. http://faostat.fao.org/site/339/default.aspx, accessed 06.07.2015.

803   Flesland, S., Hansen, K.-E., 2015. The meat product market (In Norwegian), Flesland

804   Markedsinformasjoner AS, http://flesland-markedsinfo.no/kjottvarer, accessed 06.07.2015.

805   Gjerstad, T.B., Lien, T.K., Buljo, J.O., 2006. Handle of Non-Rigid Products using a Compact

806   Needle Gripper. 39th CIRP International Seminar on Manufacturing Systems. Ljubljana,

807   Slovenia.

808   Gjerstad, T. 2012. Automated handling in fish packaging. PhD Thesis. Norwegian University of

809   Science and Technology. ISBN 978-82-471-3551-8, pp. 142-147.

810   Guire, G., Sabourin, L., Gogu, G., Lemoine, E., 2010. Robotic cell for beef carcass primal cutting

811   and pork ham boning inmeat industry. Industrial Robot: An International Journal. 37, 532–541.

812   Hinrichsen, L., 2010. Manufacturing technology in the Danish pig slaughter industry. Meat

813   Science. 84(2):271-275.

814   Hu, P.A., Bailey, J., Mathews, M., McMurray, G., Daley, W.D.R. 2012. Intelligent automation of

815   bird deboning. IEEE/ASME International Conference on Advanced Intelligent Mechatronics,

816   Kaohsiung, Taiwan, IEEE/ASME.

817   Itoh, A., Mori, Y., Sugiyama, Y., Mammoto, S., 2009. Intelligent Cutter for Pork Deboning

818   Robot-Automatic Processing of Complete Pre-Deboning Process of Pork Arm. Journal of

819   Robotics and Mechatronics. 21(3), 2.

820   Kinect Calibration. http://wiki.ros.org/kinect_calibration/technical, accessed 07.08.2015.

821 Lachat, E., Macher, H., Mittet, M.-A. Landes, T., Grussenmeyer, P., 2015. First experiences with

822 Kinect v2 sensor for close range 3D modelling. Proceedings of the International Archives of the

823 Photogrammetry, Remote Sensing and Spatial Information Sciences, Volume XL-5/W46th,

824 Avila, Spain, pp. 93-100.

825 Lien, T.K., Gjerstad, T.B., 2008. A new reversible thermal flow gripper for non-rigid products.

826 Transactions of NAMRI/SMR. 36, 565–572

827 Lippiello, V., Siciliano, B., Villani, L., 2007. Position-Based Visual Servoing in Industrial

828 Multirobot Cells Using a Hybrid Camera Configuration. IEEE Transactions on Robotics. 23(1),

829 73-86.

830 McMurray, G., 2013. Robotics and automation in the poultry industry: current technology and

831 future trends. In: Caldwell, D.G. (Eds.), Robotics and Automation in the Food Industry.

832 Woodhead Publishing Limited, Cambridge, pp. 329-353.

833 OpenCV library. Open source library for Computer Vision. www.opencv.org.

834 Paluchowski, L.A., Misimi, E., Grimsmo, L., Randeberg, L.L. 2015. Towards Automated Sorting

835 of Atlantic Cod (Gadus morhua) Roe, Milt, and Liver – Spectral characterization and

836 classification using visible and near-infrared hyperspectral imaging. Food Control.

837 http://dx.doi.org/10.1016/j.foodcont.2015.11.004

838 Park, F.C., Martin, B.J., 1994. Robot sensor calibration: solving AX= XB on the Euclidean group.

839 IEEE Transactions on Robotics and Automation. 10(5), 717-721.

840 Pettersson, A., Ohlsson, T., Davis, S., Gray, J.O., Dodd, T.J., 2011. A hygienically designed force

841 gripper for flexible handling of variable and easily damaged natural food products. Innovative

842 Food Science & Emerging Technologies. 12(3), 344-351.

843 Pieters, R., Alvarez-Aguirre, A., Jonker, P., Nijmeijer, H., 2012. Feed forward visual servoing for

844 object exploration. Proceedings of IEEE/RSJ International Conference on Intelligent Robots and

845 Systems (IROS), pp. 1702 – 1707.

846 Premaratne, P., 2014. Human Computer Interaction Using Hand Gestures. Springer, Heidelberg,

847 p. 36.

848 Purnell, G., 2013. Robotics and automation in meat processing. In: Caldwell, D.G. (Eds.),

849 Robotics and Automation in the Food Industry. Woodhead Publishing Limited, Cambridge, pp.

850 304-328.

851 Purnell, G., 2006. Automation for the Modern Slaughterhouse. In Nolet, L.M.L., Toldra, F. (Eds.)

852 Advanced Technologies for Meat Processing, CRC Press.

853 Sam, R., Nefti, S., 2010. A new design approach of robotic gripper for reducing operating cost for

854 handling food product. In Proceedings of IEEE 9th International Conference on Cybernetic

855 Intelligent Systems. Reading, UK, IEEE, 1-5.

856 Seliger, G., Szimmat, F., Niemeiet, J. Stephan, J., 2007. Automated Handling of Non-Rigid Parts,

857 Annals of the CIRP 52(1), 21-24.

858 Tsai, R.Y., Lenz, R.K., 1989. A new technique for fully autonomous and efficient 3D robotics

859 hand/eye calibration. IEEE Transactions on Robotics and Automation. 5(3), 345-358.

860 VISP- Open source library for visual tracking and visual servoing.

861 http://www.irisa.fr/lagadic/visp/download.html

862 Wolfram Rodrigues Rotation Formula,

863 http://mathworld.wolfram.com/RodriguesRotationFormula.html, accessed 24.08.2015.

864 Yang, L., Zhang, L., Dong, H., Alelaiwi, A., El Saddik, A. 2015. Evaluating and Improving the

865 Depth Accuracy of Kinect for Windows v2. IEEE Sensors Journal 15(8): 4275-4285.

866 Zhang, Z., 2000. A Flexible New Technique for Camera Calibration. IEEE Transactions on

867 Pattern Analysis and Machine Intelligence, 22(11), 1330-1334.

868 Zhou, D., Holmes, J., Holcombe, W., Lee, K.M., McMurray, G., 2007. Automation of Bird Front

869 Half Deboning Procedure: Design and Analysis. In Proceedings of the 12th IFToMM World

870 Congresses in Mechanism and Machine Science. Besançon (France).

871 Zhou, D., Daley, W., McMurray, G., 2009. Kinematics and Verification of a Deboning Device. In

872 Proceedings of the International Conference on Mechatronics and Automation (ICMA 2009),

873 2143-2148.